*Bam*H1-restricted pPR23-1 (ref. 28). Similarly, a 2.3-kb fragment was amplified using sense (5′-ATAAGAATGCGGCCGCGTGTGTCGAGCAATATCGACAG-3′) and antisense (5′-GGACTAGTCCAGAGCCACTACCGTGAGCAAG-3′) primers specific for the H37Rv *mmpL7* gene, digested with *Not*I, *Spe*I and cloned into pcDNA2.1 (Invitrogen). A 1.3-kb *Not*I fragment containing the hygromycin cassette of pHint[29] was then inserted into the *Sma*I site of the *mmpL7* fragment. The 3.6-kb *Not*I/*Spe*I fragment containing *mmpL7::hyg* was excised from pcDNA2.1 and inserted into the same sites of pPR23-1 (ref. 28). Transformation and selection procedures were as described previously[28]. To generate *attB::pks1-15*, we initially sub-cloned a 6.5-kb *Xba*I/*Xmn*I fragment containing *pks1-15* from the appropriate H37RV BAC clone (provided by R. Brosch) into *Eco*RV/*Xba*I-restricted pBluescript II SK (Stratagene). The resultant plasmid was digested with *Not*I/*Bam*H1 into which the HN878 *pks15* sequence (including the *pks1-15* junction) generated by polymerase chain reaction (PCR) was inserted. The entire *pks1-15* insert was excised with *Dra*I/*Hind*III, cloned into pMV361 (ref. 25) and transformed into HN878 *pks1-15::hyg*.

Biochemical analysis

Cultures were grown to an absorbance of 0.25 at 650 nm (A_{650}) at which point 0.1 μCi ml^{-1} [1-^{14}C]propionic acid or 0.7 μCi ml^{-1} [ring-^{14}C(U)]4-hydroxybenzoic acid (American Radiolabelled Chemicals) were added and incubated for a further 48 and 96 h, respectively. Cell pellets were re-suspended in MeOH:0.3% NaCl (aq.) (10:1) and apolar lipids extracted twice with petroleum ether as described[30]. Filtered (0.2 μM) culture supernatants were extracted twice with 0.5 volumes of petroleum ether. Lipid extracts were analysed on Silica Gel-60 TLC plates (Merck) and developed in $CHCl_3$:MeOH (94:6). For two-dimensional TLC, plates were developed in $CHCl_3$:MeOH (95:5) (1st dimension) and toluene:acetone (70:30) (2nd dimension). TLC plates were visualized using a Storm 860 PhosphorImager (Molecular Dynamics). For *in vitro* studies, approximately 1 mg of PGL was extracted and purified from 2-l cultures of HN878 by preparative Silica Gel TLC. One-dimensional ^{1}H-NMR spectroscopy was carried out on the purified material using a Mercury 300 MHz instrument and VNMR 6.1c software (Varian) with $CDCl_3$ as solvent and tetramethylsilane as an internal reference.

Animal studies

Before infection, *M. tuberculosis* cultures were adjusted to A_{650} of 0.5 and stored at −70 °C as 20% glycerol stocks. Inocula were prepared by diluting these stocks to 4×10^6 c.f.u. ml^{-1} in PBS/Tween-80 (0.05%). Six-week-old B6D2 F_1 (C57BL/6 × DBA/2; F_1 progeny) mice (Taconic) were infected (30 mice per group) via aerosol for 10 min using a BioAerosol Nebulizing Generator (CH Technologies). In this manner, approximately 50–100 c.f.u. per lung were implanted as confirmed by homogenizing lungs (4 mice per group) in 7H9/ADC at 3 h after infection and plating for c.f.u. determination. Additional mice were killed at 2, 5 and 12 weeks after infection and serial dilutions of lung and spleen homogenates were plated. The log-rank test was used to determine statistical significance of survival differences observed in mice (GraphPad Prism v3.0).

Cytokine analysis

To generate BMMs, bone marrow flushed from mouse femurs (B6D2 F_1) was cultured for 7 days in high glucose DMEM (Gibco) supplemented with 20% FCS, 1 mM pyruvate, 2 mM glutamine and 30% L929 conditioned medium. 10^6 BMMs (in high glucose DMEM plus 10% FCS, 1 mM pyruvate and 2 mM glutamine) seeded into 24-well plates were infected with various *M. tuberculosis* strains at a ratio of 1:1 for 4 h after which extracellular bacteria were removed by repeated washing with PBS. Culture supernatants were removed 18–24 h after infection, centrifuged and analysed for the presence of TNF-α, IL-6, IL-12 and MCP-1 by enzyme-linked immunosorbent assay (ELISA) (R&D Systems). Infected cells were lysed with 0.025% SDS and serial dilutions plated for c.f.u. determinations. Purified PGL (1 μg or 10 μg) and crude apolar lipid extracts (5 μg) prepared from HN878 *pks1-15::hyg* or H37Rv were re-suspended in petroleum ether, added to 24-well tissue culture plates and the solvent allowed to evaporate before adding BMMs as above. Additionally, similar assays were carried out in the presence of purified PDIM or *M. bovis* (BCG) PGL. Each infection or lipid treatment was performed in triplicate with macrophages prepared from at least three individual mice.

Received 7 May; accepted 13 July 2004; doi:10.1038/nature02837.

1. Tiruviluamala, P. & Reichman, L. B. Tuberculosis. *Annu. Rev. Publ. Health* **23,** 403–426 (2002).
2. Sreevatsan, S. *et al.* Restricted structural gene polymorphism in the *Mycobacterium tuberculosis* complex indicates evolutionarily recent global dissemination. *Proc. Natl Acad. Sci. USA* **94,** 9869–9874 (1997).
3. Fleischmann, R. D. *et al.* Whole-genome comparison of *Mycobacterium tuberculosis* clinical and laboratory strains. *J. Bacteriol.* **184,** 5479–5490 (2002).
4. North, R. J., Ryan, L., LaCource, R., Mogues, T. & Goodrich, M. E. Growth rate of mycobacteria in mice as an unreliable indicator of mycobacterial virulence. *Infect. Immun.* **67,** 5483–5485 (1999).
5. Manca, C. *et al. Mycobacterium tuberculosis* CDC1551 induces a more vigorous host response *in vivo* and *in vitro*, but is not more virulent than other clinical isolates. *J. Immunol.* **162,** 6740–6746 (1999).
6. Manca, C. *et al.* Virulence of a *Mycobacterium tuberculosis* clinical isolate in mice is determined by failure to induce Th1 type immunity and is associated with induction of IFN-α/β. *Proc. Natl Acad. Sci. USA* **98,** 5752–5757 (2001).
7. Valway, S. E. *et al.* An outbreak involving extensive transmission of a virulent strain of *Mycobacterium tuberculosis*. *N. Engl. J. Med.* **338,** 633–639 (1998).
8. Bifani, P. J., Mathema, B., Kurepina, N. E. & Kreiswirth, B. N. Global dissemination of the *Mycobacterium tuberculosis* W-Beijing family strains. *Trends Microbiol.* **10,** 45–52 (2002).
9. Glynn, J. R., Whiteley, J., Bifani, P. J., Kremer, K. & van Soolingen, D. Worldwide occurrence of Beijing/W strains of *Mycobacterium tuberculosis*: a systematic review. *Emerg. Infect. Dis.* **8,** 843–849 (2002).
10. Cole, S. T. *et al.* Deciphering the biology of *Mycobacterium tuberculosis* from the complete genome sequence. *Nature* **393,** 537–544 (1998).
11. Manca, C. *et al.* Differential monocyte activation underlies strain specific *M. tuberculosis* pathogenesis. *Infect. Immun.* (in the press).
12. Cox, J. S., Chen, B., McNeil, M. & Jacobs, W. R. Jr Complex lipid determines tissue-specific replication of *Mycobacterium tuberculosis* in mice. *Nature* **402,** 79–83 (1999).
13. Sirakova, T. D., Thirumala, A. K., Dubey, V. S., Sprecher, H. & Kolattukudy, P. E. The *Mycobacterium tuberculosis* pks2 gene encodes the synthase for the hepta- and octamethyl-branched fatty acids required for sulfolipid synthesis. *J. Biol. Chem.* **276,** 16833–16839 (2001).
14. Constant, P. *et al.* Role of the *pks15/1* gene in the biosynthesis of phenolglycolipids in the *Mycobacterium tuberculosis* complex. Evidence that all strains synthesize glycosylated p-hydroxybenzoic methly esters and that strains devoid of phenolglycolipids harbor a frameshift mutation in the *pks15/1* gene. *J. Biol. Chem.* **277,** 38148–38158 (2002).
15. Marmiesse, M. *et al.* Macro-array and bioinformatic analyses reveal mycobacterial 'core' genes, variation in the ESAT-6 gene family and new phylogenetic markers for the *Mycobacterium tuberculosis* complex. *Microbiol.* **150,** 483–496 (2004).
16. Kolattukudy, P. E., Fernandes, N. D., Azad, A. K., Fitzmaurice, A. M. & Sirakova, T. D. Biochemistry and molecular genetics of cell-wall lipid biosynthesis in mycobacteria. *Mol. Microbiol.* **24,** 263–270 (1997).
17. Vergne, I. I. & Daffe, M. Interaction of mycobacterial glycolipids with host cells. *Front. Biosci.* **3,** 865–876 (1998).
18. Hunter, S. W. & Brennan, P. J. A novel phenolic glycolipid from *Mycobacterium leprae* possibly involved in immunogenicity and pathogenicity. *J. Bacteriol.* **147,** 728–735 (1981).
19. Mehra, V., Brennan, P. J., Rada, E., Convit, J. & Bloom, B. R. Lymphocyte suppression in leprosy induced by unique *M. leprae* glycolipid. *Nature* **308,** 194–196 (1984).
20. Fournie, J.-J., Adams, E., Mullins, R. J. & Basten, A. Inhibition of human lymphoproliferative responses by mycobacterial phenolic glycolipids. *Infect. Immun.* **57,** 3653–3659 (1989).
21. Vachula, K., Holzer, T. J. & Andersen, B. R. suppression of monocyte oxidative responses by phenolic glycolipid 1 of *Mycobacterium leprae*. *J. Immunol.* **142,** 1696–1701 (1989).
22. Silva, C. L., Faccioli, L. H. & Foss, N. T. Suppression of human monocyte cytokine release by phenolic glycolipid-1 of *Mycobacterium leprae*. *Int. J. Lepr.* **61,** 107–108 (1993).
23. Hashimoto, K. *et al. Mycobacterium leprae* infection in monocyte-derived dendritic cells and its influence on antigen-presenting function. *Infect. Immun.* **70,** 5167–5176 (2002).
24. Ng, V. *et al.* Role of the cell wall phenolic glycolipid-1 in the peripheral nerve predilection of *Mycobacterium leprae*. *Cell* **103,** 511–524 (2000).
25. Stover, C. K. *et al.* New use of BCG for recombinant vaccines. *Nature* **351,** 456–460 (1991).
26. Gordon, S. Alternative activation of macrophages. *Nature Rev. Immunol.* **3,** 23–35 (2003).
27. Garbe, T. R. *et al.* Transformation of mycobacterial species using hygromycin resistance as selectable marker. *Microbiol.* **140,** 133–138 (1994).
28. Pelicic, V. *et al.* Efficient allelic exchange and transposon mutagenesis in *Mycobacterium tuberculosis*. *Proc. Natl Acad. Sci. USA* **94,** 10955–10960 (1997).
29. O'Gaora, P. *et al.* Mycobacteria as immunogens: development of expression vectors for use in multiple mycobacterial species. *Med. Princ. Prac.* **6,** 91–96 (1997).
30. Slayden, R. A. & Barry, C. E. III in *Mycobacterium tuberculosis protocols* (eds Parish, T. & Stoker, N. G.) 229–245 (Humana, New Jersey, 2001).

Acknowledgements The authors wish to thank J. Gonzales and M. Goodwin for their assistance with animal studies and NMR spectroscopy, respectively. G.K. is supported by grants from the NIH.

Competing interests statement The authors declare that they have no competing financial interests.

Correspondence and requests for materials should be addressed to C.E.B. (clifton_barry@nih.gov).

Involvement of targeted proteolysis in plant genetic transformation by *Agrobacterium*

Tzvi Tzfira, Manjusha Vaidya & Vitaly Citovsky

Department of Biochemistry and Cell Biology, State University of New York, Stony Brook, New York 11794-5215, USA

Genetic transformation of plant cells by *Agrobacterium* represents a unique case of trans-kingdom DNA transfer[1]. During this process, *Agrobacterium* exports its transferred (T) DNA and several virulence (Vir) proteins into the host cell[2], within which T-DNA nuclear import is mediated by VirD2 (ref. 3) and VirE2 (ref. 4) and their host cell interactors AtKAP-α[5] and VIP1 (ref. 6), whereas its integration is mediated mainly by host cell proteins[7–9].

The factors involved in the uncoating of T-DNA from its cognate proteins, which occurs before integration into the host genome, are still unknown. Here, we report that VirF—one of the few known exported Vir proteins whose function in the host cell remains unknown—is involved in targeted proteolysis of VIP1 and VirE2. We show that VirF localizes to the plant cell nucleus and interacts with VIP1, a nuclear protein. VirF, which contains an F-box motif[10], significantly destabilizes both VIP1 and VirE2 in yeast cells. Destabilization of VIP1 in the presence of VirF was then confirmed *in planta*. These results suggest that VIP1 and its cognate VirE2 are specifically targeted by the VirF-containing Skp1–Cdc53-cullin–F-box complex for proteolysis. The critical role of proteasomal degradation in *Agrobacterium*-mediated genetic transformation was also evident from inhibition of T-DNA expression by a proteasomal inhibitor.

Agrobacterium genetically transforms eukaryotic cells from diverse origins, from its natural plant hosts (reviewed in refs 8, 9) to yeast[11] to human[12]. During this process, the bacterial T-DNA is thought to be imported into the host cell nucleus as a DNA–protein complex (T-complex) composed of a single T-DNA strand packaged by numerous VirE2 molecules, a single VirD2 molecule attached to its 5′ end, and VIP1 proteins bound to VirE2 (reviewed in refs 13, 14). Before integration into the host genome, the T-DNA must be uncoated from its cognate proteins by a process yet to be determined. We suggest that this is achieved by means of targeted proteolysis mediated by the bacterial virulence protein VirF, which

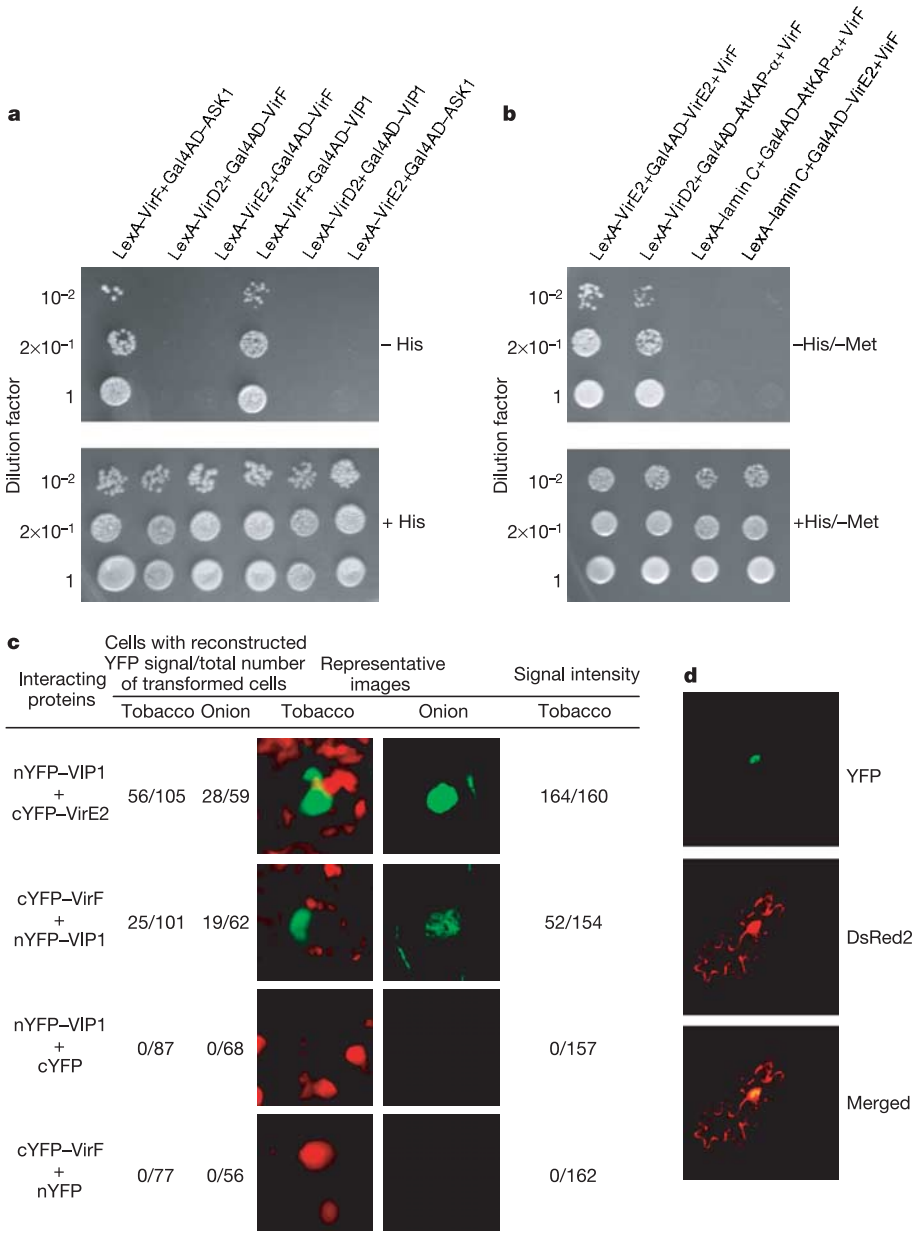

Figure 1 Specific interaction between VirF and VIP1 in yeast and plant cells. **a**, **b**, Yeast two-hybrid assay. L40(−ura3) cells were grown in histidine-deficient medium with 10 mM of 3-amino-1,2,4-triazole (−His) or in histidine-containing medium (+His); free VirF was co-expressed in the absence of methionine (−Met) from a methionine-repressible promoter. **c**, *In planta* BiFC assay. Signal intensity of reconstructed YFP (green) is presented relative to plastid autofluorescence (red). **d**, Nuclear localization of the interacting VirF and VIP1 proteins was confirmed in tobacco cells by co-localization (yellow colour in the merged image) of reconstructed YFP (yellow) with free DsRed2 (red), which labels both the cytoplasm and the nucleus[22]. All images are single confocal sections.

is exported into plant cells[2] and contains an F-box motif that binds the plant homologue of Skp1, ASK1 (ref. 10). Since its discovery as a host range factor[15–17], the molecular basis for the function of VirF has remained elusive. We reasoned that VirF might be involved in destabilization of the protein components of the T-complex by participating in a Skp1–Cdc53-cullin–F-box (SCF) complex involved in protein degradation (reviewed in ref. 18). In this model, one or more of the T-DNA-associated proteins would be recognized by VirF and represent a substrate for targeted proteolysis. Figure 1a shows that, in the yeast two-hybrid system, VirF, which also bound ASK1, specifically interacted with VIP1, but not with VirD2 or VirE2. This latter lack of interaction was not due to instability of VirE2 and VirD2 in the presence of VirF because co-expression of free VirF did not affect VirE2–VirE2 (ref. 19) and VirD2–AtKAP-α[5] interactions (Fig. 1b). VIP1, known to bind VirE2 (ref. 6), did not interact with VirD2, and no interaction between ASK1 and VirE2 was detected. Thus, of all the known T-complex protein components, VirF specifically recognizes VIP1 in yeast.

The VirF–VIP1 interaction was confirmed *in planta* using the bimolecular fluorescence complementation (BiFC) assay[20]. In this approach, the yellow fluorescent protein (YFP) molecule is split into amino-terminal (nYFP) and carboxy-terminal (cYFP) non-fluorescent portions. Restoration of the YFP fluorescence signal is achieved when nYFP and cYFP are brought together as fusions with interacting proteins[20]. Figure 1c shows that YFP fluorescence was restored in tobacco and onion cells—both of which are infected by *Agrobacterium*[21]—after co-expression of nYFP–VIP1 and cYFP–VirF, yet the intensity of the reconstructed YFP signal was weaker and the number of cells exhibiting the fluorescence signal was generally lower than those observed for the VIP1–VirE2 interaction. These differences probably reflect the biological effect of the VirF–VIP1 interaction (see below). No YFP fluorescence was detected when nYFP–VIP1 or cYFP–VirF were co-expressed with unfused cYFP or nYFP, respectively (Fig. 1c); this lack of background signal, previously reported for BiFC in animal cells[20], facilitated identification of cells exhibiting the reconstructed YFP fluorescence.

If VirF and ASK1 are involved in uncoating of the T-DNA before its expression and integration, they both should reside in the host cell nucleus where VirF would interact with its target, VIP1. Indeed, green fluorescent protein (GFP)-tagged VirF and ASK1 accumulated in the nuclei of plant cells (data not shown). Furthermore, the VirF–VIP1 complexes were also intranuclear, co-localizing with co-expressed DsRed2 (Fig. 1d), which labels both the nucleus and the cytoplasm[22].

Next, the VirF-mediated protein destabilization was assayed by a previously reported approach in which SCF-dependent protein degradation is monitored using fusions to a reporter protein; decrease in the reporter activity indicates decreased stability[23]. We examined the effect of VirF on the stability of three protein components of the T-complex (VIP1, VirE2 and VirD2) in two experimental systems: yeast and plant. In yeast, expression of GFP-tagged VIP1, VirE2 and VirD2 was controlled by a galactose-inducible promoter, whereas expression of unlabelled VirF was controlled by a methionine-repressible promoter. We compared the GFP signal (black bars in Fig. 2) produced in control systems (that is, after cell growth in galactose-containing medium) with the GFP signal (grey bars in Fig. 2) accumulated after transferring the cells to a glucose-containing medium, with or without induction of VirF expression. Figure 2a shows that VirF significantly depleted the amount of GFP–VIP1, reducing it to about 25% of its original level. No such changes in GFP signal were observed under VirF-repressing conditions (Fig. 2a), indicating the specific role of VirF in destabilization of GFP–VIP1. Furthermore, VirF expression also caused destabilization of up to 60% of GFP–VirE2 when co-expressed with free, unfused VIP1 (Fig. 2b). This destabilization was VIP1-dependent because GFP–VirE2 co-expressed with VirF in the absence of VIP1 remained stable (Fig. 2b). GFP–VirD2, which does not interact with VirF (see Fig. 1a) or VIP1 (ref. 6), was not destabilized when co-expressed with VirF and VIP1 (Fig. 2c). Note that, under our experimental conditions, the VirF-induced destabilization of VIP1 and VirE2 was incomplete, explaining why interactions between VirF and VIP1 could still be detected in the two-hybrid system and in the BiFC assay; most likely, the residual levels of these proteins were sufficient to induce expression of the two-hybrid reporter genes and to reconstruct detectable levels of the YFP signal (see Fig. 1a, c). That these low amounts of VirE2 and VIP1 still remained in the cells may be due to their *de novo* synthesis or recalcitrance of some of the expressed protein to degradation.

Because VirF is an F-box protein thought to participate in the SCF-mediated degradation[10], we directly tested whether the VirF-containing SCF (SCF^{VirF}) pathway is involved in destabilization of GFP–VIP1. To this end, we used a yeast temperature-sensitive mutant in the Skp1 component of the SCF complex, *skp1-4* (ref. 24). Figure 2d shows that VirF expressed in *skp1-4* cells substantially destabilized GFP–VIP1 at the permissive temperature (25 °C), but not after shift to the restrictive temperature (37 °C). As expected, in the parental, wild-type yeast strain, destabilization of GFP–VIP1 occurred with equal efficiency at both temperatures (not shown).

Collectively, these results suggest that VirF specifically destabilizes VIP1 and VirE2 via targeted proteolysis mediated by SCF^{VirF}. Also, because VirF binds VIP1 but not VirE2 (see Fig. 1a), its effect on VIP1 stability was probably direct whereas the stability of VirE2 was affected indirectly, presumably through the VIP1–VirE2 interaction.

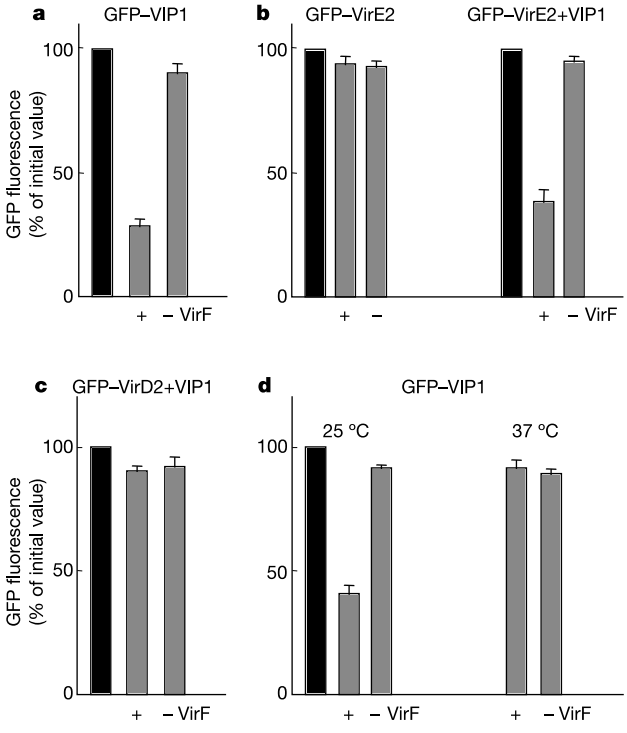

Figure 2 VirF-mediated and Skp1-dependent destabilization of VIP1 and VirE2 in yeast cells. **a**, Destabilization of GFP–VIP1. **b**, Destabilization of GFP–VirE2. **c**, Lack of destabilization of GFP–VirD2. **d**, Destabilization of GFP–VIP1 at permissive (25 °C) but not at restrictive (37 °C) temperature in *skp1-4* cells. Combinations of target genes are indicated on the top of each panel, and initial levels of GFP fluorescence, measured after induction of the target proteins in the absence of VirF expression, are indicated by black bars. Fluorescent signal measured after induction (+) or continued repression (−) of VirF is indicated by grey bars. Bars represent mean ± standard error ($n = 5$).

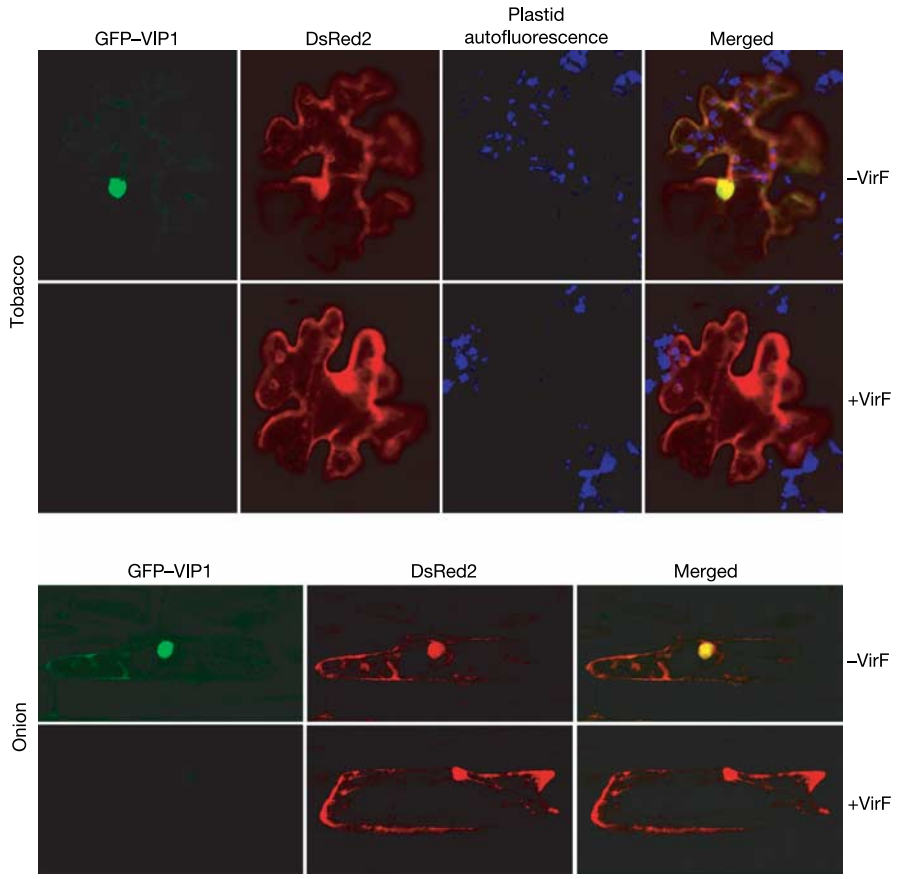

Figure 3 VirF-mediated destabilization of VIP1 *in planta*. Plant tissues were transiently transformed with pGDR–GFP–VIP1 alone or mixed with pRTL2–VirF. pGDR–GFP–VIP1 expresses both GFP–VIP1 and free DsRed2 whereas pRTL2–VirF expresses unfused VirF. DsRed2 labels the cytoplasm and the nucleus and identifies transformed cells. GFP, green; DsRed2, red; co-localizing merged GFP and DsRed2, yellow; plastid autofluorescence, blue. All images are single confocal sections.

The effect of VirF on VIP1 stability was then examined directly *in planta* by transiently co-expressing GFP–VIP1 and free VirF. The DsRed2 fluorescent marker, located on the same plasmid that expressed GFP–VIP1, was used to identify the transformed cells and to visualize their nucleus and cytoplasm, between which it is known to partition[22]. As expected[6,25], in the absence of VirF, VIP1 predominantly accumulated in the nuclei of tobacco and onion cells (Fig. 3). In the presence of VirF, however, a significant population of the transformed cells displayed no GFP–VIP1 signal, but still accumulated the DsRed2 fluorescence (Fig. 3). Thus, although the DsRed2/GFP–VIP1-encoding construct had been delivered to and was expressed in these cells, GFP–VIP1 was depleted to levels below our detection limits. In addition, consistent with the reconstructed but weak fluorescence signal in the BiFC experiments (see Fig. 1c, d), low, residual levels of GFP–VIP1 fluorescence could still be observed in some cells co-expressing GFP–VIP1 and VirF (not shown). These data suggest that, in plant cells, the presence of VirF destabilizes VIP1, potentially through the SCF^{VirF} pathway. Owing to technical difficulties with reproducible expression of three co-bombarded constructs, we were unable to examine the effect of VirF on the stability of VirE2 in the presence of overexpressed VIP1.

To examine the effect of the 26S proteasome on T-DNA expression, tobacco tissues were treated with the proteasome inhibitor MG132 (ref. 26) for 2 h before and during the first 2 h of their inoculation with *Agrobacterium*, and T-DNA expression was monitored by polymerase chain reaction with reverse transcription (RT–PCR)[27]. Figure 4a shows that, in untreated leaf disks, T-DNA-specific transcripts were detected already 2 h after inoculation, and that addition of DMSO, the MG132 solvent, to the incubation medium did not alter the efficiency and the pattern of T-DNA expression.

In contrast, RT–PCR analysis of the MG132-treated disks detected the T-DNA-specific products significantly later, 6–8 h after inoculation (Fig. 4a). This inhibitory effect of MG132 on T-DNA expression was observed with both concentrations (25 μM and 50 μM) of the proteasome inhibitor used in our experiments, with the higher amount of MG132 being slightly more effective (Fig. 4a). Thus, MG132 affected T-DNA expression early in the infection process. This inhibition of T-DNA expression was specific, as MG132 had no discernible effect on expression of genes introduced into plant tissues by an *Agrobacterium*-independent method. Indeed, Fig. 4b shows that no differences in expression of the *gfp* gene were detected when this gene was bombarded into untreated leaf disks, or into disks treated with DMSO or with 25 μM or 50 μM of MG132, indicating that MG132 did not simply interfere with the gene expression ability of the plant cell. Although the effect of MG132 on T-DNA expression may still be also due to other, more indirect effects on the plant cell, these results, taken together with VirF-induced destabilization of VirE2 and VIP1, strongly suggest involvement of proteasomal degradation in *Agrobacterium*-mediated genetic transformation.

VirE2 is thought to package the transported T-DNA molecule into a T-complex, protect it and, together with the host factor VIP1, assist its nuclear import (reviewed in refs 13, 14). Thus, disassembly of the T-complex of VirE2 and VIP1 probably occurs within the nucleus, before integration. Our data provide direct evidence for the role of VirF in intranuclear proteolysis of two of the protein components of the *Agrobacterium* T-complex—VIP1 and VirE2—

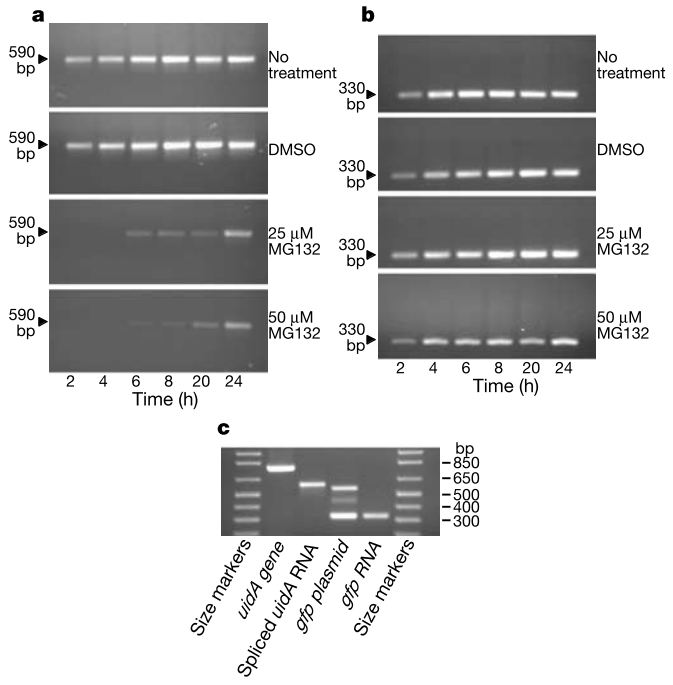

Figure 4 The effect of 26S proteasome inhibition on T-DNA expression. **a**, **b**, RT–PCR analysis of T-DNA (**a**) and bombarded *gfp* (**b**) expression in MG132-treated leaf disks. **c**, Control PCR reactions. T-DNA expression was detected using *uidA*-specific primers that yield a 590-base-pair (bp) PCR product for the spliced *uidA* transcript and a 779-bp PCR product for the intron-containing *uidA* sequence. *gfp* expression was detected using *gfp*-specific primers, in combination with a third primer located within the promoter of the *gfp* gene, that yield a 330-bp PCR product for the *gfp* transcript and a 560-bp PCR product for the *gfp* promoter-containing plasmid sequences.

via the SCF^{VirF}-mediated pathway. This notion is supported by our observations that early expression of T-DNA, which requires uncoating of the T-complex, is largely blocked by an inhibitor of the 26S proteasome. Interestingly, as a host range factor, VirF is required for transformation of some but not all plant species[15–17,28,29]. Thus, in plants that do not require VirF, its function may be fulfilled by an as yet unidentified nuclear-localized cellular F-box protein; indeed, many other pathogenic bacteria export to their eukaryotic hosts proteins that mimic functions of the host cell factors required for the infection (reviewed in ref. 30). □

Methods

BiFC assay for protein–protein interaction *in planta*

VIP1, VirE2 and VirF were fused to the C terminus of either the 5′ half (nYFP) or the 3′ half (cYFP) of the YFP open reading frame dissected between codons 154 and 155 (ref. 20). Different combinations of the tested proteins were mixed and co-bombarded into tobacco leaves or onion scales. Transformation efficiency was estimated by parallel bombardment of full-length YFP. Signal intensity of reconstructed YFP is presented relative to plastid autofluorescence by calculating the green to red pixel ratio between ten transfected cells with reconstructed YFP signal and an average of 20 randomly chosen plastids from each transfected cell and its surrounding cells. For subcellular localization of the VirF–VIP1 complexes, nYFP–VIP1 and free DsRed2 were expressed from a single plasmid by cloning a 35S promoter–nYFP–VIP1–35S terminator cassette into pGDR[22] that already contained the *dsred2* gene under a constitutive promoter, resulting in pGDR–nYFP–VIP1, which was then co-bombarded with cYFP–VirF into tobacco leaves.

Protein destabilization assay in yeast

VIP1, VirE2, or VirD2 fused to the C terminus of GFP, as well as free VIP1, were expressed from the galactose-inducible promoter and free VirF was expressed from the methionine repressible promoter. TAT7 yeast cells, carrying the indicated plasmid combinations, were grown overnight at 30 °C in selective minimal medium with glucose (10% final concentration), washed, and diluted to $A_{600} = 0.1$. For induction of expression, cell cultures were supplemented with galactose (10% final concentration) and allowed to grow for 3 h at 30 °C. At this time, the cells were sampled to determine their GFP fluorescence; this signal represented the initial level of the GFP-tagged protein accumulated in the expressing cells. The remaining cultures was then collected, washed, and transferred to a glucose-containing growth medium, which either lacked methionine for induction of VirF expression or contained methionine for continuing suppression of VirF synthesis. Three hours later, GFP fluorescence in the live cell cultures was determined, and destabilization of the GFP-tagged proteins was estimated from the reduction in GFP fluorescence calculated as per cent of the initial signal level.

For inactivation of Skp1, the temperature-sensitive *skp1-4* cells, which arrest in the cell cycle[24], were maintained at the permissive temperature (25 °C) during overnight growth and galactose induction, and shifted to the restrictive temperature (37 °C) for methionine depletion.

Protein destabilization assay *in planta*

gfp–VIP1 was cloned into pGDR, and unfused *virF* was cloned into pRTL2, producing pGDR–GFP–VIP1 and pRTL2–VirF, respectively. pGDR–GFP–VIP1 alone or mixed with pRTL2–VirF (1:1 mol/mol) was bombarded into tobacco leaves or onion scales, and the expression patterns of GFP and DsRed2 were analysed by confocal microscopy. Cells transformed with pGDR–GFP–VIP1 were identified by the presence of DsRed2 whereas VIP1 degradation in these cells was determined by reduction or disappearance of the GFP fluorescence.

Early T-DNA expression assay in the presence of MG132

To detect specifically T-DNA expressed in plants, but not in *Agrobacterium*, we chose the binary plasmid pBIG–HYG–GUS that carries in its T-DNA an intron-containing *uidA* gene, the transcript of which is spliced only within plant cells. Tobacco leaf disks were placed on a regeneration medium supplemented with MG132 (25 μM or 50 μM in 1% DMSO), incubated for 2 h at 25 °C, bombarded with a GFP-expressing plasmid (pRTL2–GFP), and immediately inoculated with acetosyringone-induced culture (final $A_{600} = 1.5$) of *Agrobacterium* strain EHA105 harbouring pBIG–HYG–GUS. The incubation was continued for 2 h, after which the leaf disks were washed, transferred to a fresh regeneration medium, and sampled at 2, 4, 6, 8, 20 and 24 h after inoculation. Expression of the T-DNA and of the bombarded pRTL2–GFP was analysed by RT–PCR as described[27], using *uidA*- and *gfp*-specific primers.

Received 23 April; accepted 12 July 2004; doi:10.1038/nature02857.

1. Stachel, S. E. & Zambryski, P. C. Generic trans-kingdom sex? *Nature* **340,** 190–191 (1989).
2. Vergunst, A. C. *et al.* VirB/D4-dependent protein translocation from *Agrobacterium* into plant cells. *Science* **290,** 979–982 (2000).
3. Howard, E., Zupan, J., Citovsky, V. & Zambryski, P. C. The VirD2 protein of *A. tumefaciens* contains a C-terminal bipartite nuclear localization signal: implications for nuclear uptake of DNA in plant cells. *Cell* **68,** 109–118 (1992).
4. Citovsky, V., Zupan, J., Warnick, D. & Zambryski, P. C. Nuclear localization of *Agrobacterium* VirE2 protein in plant cells. *Science* **256,** 1802–1805 (1992).
5. Ballas, N. & Citovsky, V. Nuclear localization signal binding protein from *Arabidopsis* mediates nuclear import of *Agrobacterium* VirD2 protein. *Proc. Natl Acad. Sci. USA* **94,** 10723–10728 (1997).
6. Tzfira, T., Vaidya, M. & Citovsky, V. VIP1, an *Arabidopsis* protein that interacts with *Agrobacterium* VirE2, is involved in VirE2 nuclear import and *Agrobacterium* infectivity. *EMBO J.* **20,** 3596–3607 (2001).
7. Tzfira, T., Li, J., Lacroix, B. & Citovsky, V. *Agrobacterium* T-DNA integration: molecules and models. *Trends Genet.* **20,** 375–383 (2004).
8. Gelvin, S. B. *Agrobacterium*-mediated plant transformation: the biology behind the "gene-jockeying" tool. *Microbiol. Mol. Biol. Rev.* **67,** 16–37 (2003).
9. Gelvin, S. B. *Agrobacterium* and plant genes involved in T-DNA transfer and integration. *Annu. Rev. Plant Physiol. Plant Mol. Biol.* **51,** 223–256 (2000).
10. Schrammeijer, B. *et al.* Interaction of the virulence protein VirF of *Agrobacterium tumefaciens* with plant homologs of the yeast Skp1 protein. *Curr. Biol.* **11,** 258–262 (2001).
11. Bundock, P., den Dulk-Ras, A., Beijersbergen, A. & Hooykaas, P. J. J. Trans-kingdom T-DNA transfer from *Agrobacterium tumefaciens* to *Saccharomyces cerevisiae*. *EMBO J.* **14,** 3206–3214 (1995).
12. Kunik, T. *et al.* Genetic transformation of HeLa cells by *Agrobacterium*. *Proc. Natl Acad. Sci. USA* **98,** 1871–1876 (2001).
13. Zupan, J., Muth, T. R., Draper, O. & Zambryski, P. C. The transfer of DNA from *Agrobacterium tumefaciens* into plants: a feast of fundamental insights. *Plant J.* **23,** 11–28 (2000).
14. Tzfira, T. & Citovsky, V. Partners-in-infection: host proteins involved in the transformation of plant cells by *Agrobacterium*. *Trends Cell Biol.* **12,** 121–129 (2002).
15. Melchers, L. S. *et al.* Octopine and nopaline strains of *Agrobacterium tumefaciens* differ in virulence; molecular characterization of the *virF* locus. *Plant Mol. Biol.* **14,** 249–259 (1990).
16. Jarchow, E., Grimsley, N. H. & Hohn, B. *virF*, the host range-determining virulence gene of *Agrobacterium tumefaciens*, affects T-DNA transfer to *Zea mays*. *Proc. Natl Acad. Sci. USA* **88,** 10426–10430 (1991).
17. Regensburg-Tuink, A. J. & Hooykaas, P. J. J. Transgenic *N. glauca* plants expressing bacterial virulence gene virF are converted into hosts for nopaline strains of *A. tumefaciens*. *Nature* **363,** 69–71 (1993).
18. del Pozo, J. C. & Estelle, M. F-box proteins and protein degradation: an emerging theme in cellular regulation. *Plant Mol. Biol.* **44,** 123–128 (2000).
19. Deng, W. *et al.* VirE1 is a specific molecular chaperone for the exported single-stranded-DNA-binding protein VirE2 in *Agrobacterium*. *Mol. Microbiol.* **31,** 1795–1807 (1999).
20. Hu, C. D., Chinenov, Y. & Kerppola, T. K. Visualization of interactions among bZIP and Rel family proteins in living cells using bimolecular fluorescence complementation. *Mol. Cell* **9,** 789–798 (2002).
21. Dommisse, E. M., Leung, D. W. M., Shaw, M. L. & Conner, A. J. Onion is a monocotyledonous host for *Agrobacterium*. *Plant Sci.* **69,** 249–257 (1990).
22. Goodin, M. M., Dietzgen, R. G., Schichnes, D., Ruzin, S. & Jackson, A. O. pGD vectors: versatile tools for the expression of green and red fluorescent protein fusions in agroinfiltrated plant leaves. *Plant J.* **31,** 375–383 (2002).

23. Gray, W. M., Kepinski, S., Rouse, D., Leyser, O. & Estelle, M. Auxin regulates SCF^{TIR1}-dependent degradation of AUX/IAA proteins. *Nature* **414,** 271–276 (2001).
24. Connelly, C. & Hieter, P. Budding yeast *SKP1* encodes an evolutionarily conserved kinetochore protein required for cell cycle progression. *Cell* **86,** 275–285 (1996).
25. Tzfira, T., Vaidya, M. & Citovsky, V. Increasing plant susceptibility to *Agrobacterium* infection by overexpression of the *Arabidopsis VIP1* gene. *Proc. Natl Acad. Sci. USA* **99,** 10435–10440 (2002).
26. Lee, D. H. & Goldberg, A. L. Proteasome inhibitors: valuable new tools for cell biologists. *Trends Cell Biol.* **8,** 397–403 (1998).
27. Narasimhulu, S. B., Deng, X.-B., Sarria, R. & Gelvin, S. B. Early transcription of *Agrobacterium* T-DNA genes in tobacco and maize. *Plant Cell* **8,** 873–886 (1996).
28. Otten, L. *et al.* Restoration of virulence of *vir* region mutants of *A. tumefaciens* strain B6S3 by coinfection with normal and mutant *Agrobacterium* strains. *Mol. Gen. Genet.* **195,** 159–163 (1984).
29. Schrammeijer, B., Hemelaar, J. & Hooykaas, P. J. The presence and characterization of a *virF* gene on *Agrobacterium vitis* Ti plasmids. *Mol. Plant Microbe Interact.* **11,** 429–433 (1998).
30. Nagai, H. & Roy, C. R. Show me the substrates: modulation of host cell function by type IV secretion systems. *Cell. Microbiol.* **5,** 373–383 (2003).

Acknowledgements We thank S. Gelvin for VirF and *Agrobacterium* strains, T. Durfee for ASK1, and M. Goodin for pGDR. We are also grateful to R. Sternglanz and A. Neiman for their suggestions and discussion. The work in our laboratory is supported by grants from the National Institutes of Health, National Science Foundation, US Department of Agriculture, US–Israel Bi-national Science Foundation (BSF), and US–Israel Bi-national Agricultural Research and Development Fund (BARD) to V.C., and by grants from BARD and Human Frontiers Science Program to T.T.

Competing interests statement The authors declare that they have no competing financial interests.

Correspondence and requests for materials should be addressed to T.T. (ttzfira@ms.cc.sunysb.edu).

Centrosomes direct cell polarity independently of microtubule assembly in *C. elegans* embryos

Carrie R. Cowan & Anthony A. Hyman

Max Planck Institute of Molecular Cell Biology and Genetics, Pfotenhauerstrasse 108, Dresden 01307, Germany

Polarity establishment requires a symmetry-breaking event, resulting in an axis along which determinants are segregated. In *Caenorhabditis elegans*, oocytes are apolar and are triggered to polarize rapidly along one axis after fertilization. The establishment of this first polarity axis is revealed by the asymmetric distribution of PAR proteins and cortical activity in the one-celled embryo. Current evidence suggests that the centrosome–pronucleus complex contributed by the sperm is involved in defining the polarization axis[1–6]. Here we directly assess the contribution of the centrosome to polarity establishment by laser ablating the centrosome before and during polarization. We find that the centrosome is required to initiate polarity but not to maintain it. Initiation of polarity coincides with the proximity of the centrosome to the cortex and the assembly of pericentriolar material on the immature sperm centrosome. Depletion of microtubules or the microtubule nucleator γ-tubulin did not affect polarity establishment. These results demonstrate that the centrosome provides an initiating signal that polarizes *C. elegans* embryos and indicate that this signalling event might be independent of the role of the centrosome as a microtubule nucleator.

After fertilization, the PAR proteins are uniformly distributed in the *C. elegans* embryo[5,7–9]. Coincident with the completion of female meiosis, about 30 min after fertilization, shallow ingressions ('ruffles') become visible throughout the cortex. On perception of a polarization signal a few minutes later, the PAR proteins segregate into their anterior (PAR-3 and PAR-6)[5,8,9] and posterior (PAR-1 and PAR-2)[5,7,10] domains. Concomitantly, contractile polarity is established[5]: the anterior cortex continues to ruffle while cortical activity in the posterior ceases, creating a smooth domain. The male pronucleus and microtubule asters lie adjacent to the smooth, posterior PAR-2 domain[5,6]. To investigate when centrosome–cortex proximity occurs relative to the initiation of polarity, centrosome position was monitored with a green fluorescent protein (GFP)-tagged centrosome marker, SPD-2 (ref. 11), and polarity was assessed both by GFP–PAR-2 (Fig. 1a; Supplementary Movie 1) and by cortical ruffling. The initiation of cortical polarity was evident as a progressive cessation of ruffling, spreading from a focus on the cortex, and within 2 min GFP–PAR-2 was visible on the expanding smooth cortex. Before the onset of polarization, the centrosome–cortex distances were variable (Fig. 1b; the range at −3:20 (3 min 20 s before the onset of posterior smoothing) was 0–9 μm; $n = 9$). However, we consistently observed that the centrosome was closest to the cortex when cortical polarity was initiated (Fig. 1b; range at 0:00 was 0–4 μm; $n = 14$). Thus, polarity initiation coincided with centrosome–cortex proximity.

As a direct test of the role of the centrosome in polarity establishment, centrosomes were located during female meiosis with the use of GFP–SPD-2 fluorescence and the labelled centrosomes were ablated with a pulsed ultraviolet-laser microbeam. Polarity was assessed by time-lapse imaging of GFP–PAR-2 or contractile polarity. Successful ablations were judged by the absence of a GFP–SPD-2 structure throughout the recording period (minimally 30 min after ablation) and a failure of the fast phase of pronuclear migration, a phenotype associated with centrosome defects. In embryos in which the centrosome was successfully ablated before the onset of polarity, no asymmetric PAR-2 localization was observed ($n = 30$; Fig. 2a; Supplementary Movies 2 and 3) and ruffling continued throughout the entire cortex (Supplementary

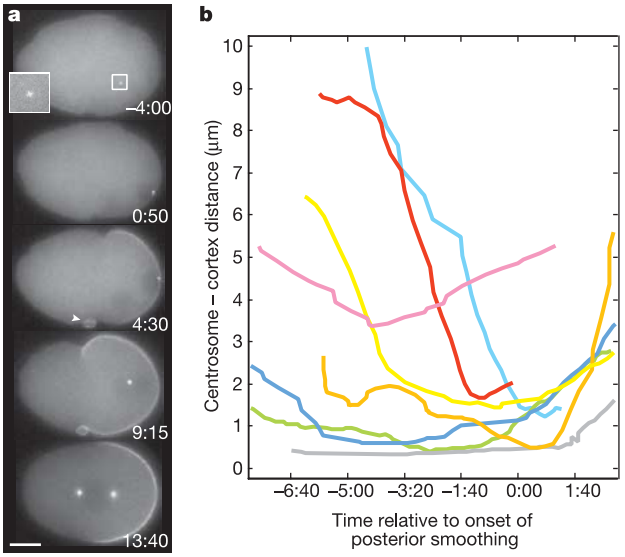

Figure 1 The centrosome lies adjacent to the cortex at the time of polarity initiation. **a**, Time lapse images of a GFP–PAR-2; GFP–SPD-2 embryo (Supplementary Movie 1). The GFP–SPD-2-labelled centrosome is visible as a bright cytoplasmic dot (the second centrosome is out of the focal plane); GFP–PAR-2 labels the posterior cortex. The small ring of GFP–PAR-2 (arrowhead, 4:30) corresponds to the polar body cortex. The embryo posterior is to the right. Scale bar, 10 μm. **b**, Centrosome–cortex distances during polarity establishment. Solid lines indicate the distance (μm) from the centrosome to the nearest point on the cortex over time. PAR-2 polarity was established at about 2:00 (see Methods). Times were standardized to the onset of posterior smoothing, indicating polarity establishment. Only a subset of experiments is shown.